

Rethinking Orbital Imaging

Establishing Guidelines for Interpreting Orbital Imaging Studies and Evaluating Their Predictive Value in Patients with Orbital Tumors

Guy J. Ben Simon, MD,¹ Christine C. Annunziata, MD,¹ James Fink, MD,² Pablo Villablanca, MD,² John D. McCann, MD, PhD,¹ Robert A. Goldberg, MD¹

Purpose: To establish guidelines for interpretation of orbital imaging by magnetic resonance imaging (MRI) and/or computed tomography (CT), and to apply these guidelines and examine their predictive value in 131 patients with biopsy-proven orbital tumors.

Design: Prospective evaluation of imaging studies.

Participants: Imaging studies (CT and/or MRI) from 131 cases with biopsy-proven orbital tumors.

Methods: Guidelines for reviewing orbital imaging studies (MRI and/or CT) were established based on 5 major characteristics: (1) anatomic location, (2) bone and paranasal sinuses involvement, (3) content, (4) shape, and (5) associated features. In total, 84 features were established by an experienced orbital surgeon and a neuroradiologist. Applying these 84 features, imaging studies of 131 biopsy-proven orbital tumors were evaluated by 3 physicians.

Main Outcome Measures: Imaging features: characteristics, sensitivity, specificity, and positive and negative predictive values in various groups of orbital tumors and κ values.

Results: One hundred thirty-one cases of biopsy-proven orbital tumors were evaluated. Benign lesions were more likely to be smaller in size, round or oval in shape (29% of all benign tumors, 0% in malignant and inflammatory, $P < 0.001$), and associated with hyperostosis (22% of all benign lesions, $P < 0.001$). They were also more likely to be hyperdense or hypodense on CT imaging (15% and 11%, respectively; $P < 0.05$ in comparison with inflammatory and malignant tumors). Inflammatory processes showed panorbital involvement (23% vs. 3%, and 0% in benign and malignant tumors, respectively; $P < 0.001$). Orbital fat involvement and fat stranding were noticed only in inflammatory lesions (19% and 16%, respectively; $P < 0.001$). None of the features occurred only in malignant tumors, but they tend to involve the anterior orbit more commonly (54% vs. 20%, and 29% in benign and malignant; $P = 0.002$), and were more likely to show bone erosion (31% vs. 6%, and 16% in benign and inflammatory tumors, respectively; $P = 0.004$) and molding around orbital structures (29% vs. 3% in benign, and 0% in inflammatory tumors, respectively; $P < 0.001$). Features such as panorbital involvement, orbital fat, frontal sinus opacity, molding around orbital structures, perineural involvement, and fat stranding had specificity of 97% to 100%, but low sensitivity.

Conclusions: Guidelines for analysis of orbital imaging studies (CT or MRI) are suggested. Based on these guidelines several imaging features showed significantly different occurrences in benign, malignant, and inflammatory processes; although this can help in differential diagnosis, tissue diagnosis may still be required. *Ophthalmology* 2005;112:2196–2207 © 2005 by the American Academy of Ophthalmology.

Originally received: April 21, 2005.

Accepted: September 8, 2005.

Manuscript no. 2005-347.

¹ Jules Stein Eye Institute and Department of Ophthalmology, Los Angeles, California.

² Division of Neuroradiology and Department of Radiology, David Geffen School of Medicine at UCLA, Los Angeles, California.

The authors have no proprietary interest in any of the materials mentioned in the article.

Correspondence to Guy J. Ben Simon, MD, The Royal Victorian Eye and Ear Hospital, 32 Gisborne Street, East Melbourne 3002, Victoria, Australia. E-mail: guybensimon@gmail.com.

Management of orbital tumors is complex and frequently requires collaborative work of physicians from different medical disciplines, including oculofacial surgery, neuroradiology, pathology, and medical and radiation oncology. Tissue diagnosis, either by open biopsy or fine needle aspiration, is considered a gold standard in the diagnosis. However, histopathological results are not always clearly definitive. Furthermore, in cases such as orbital apex or cavernous sinus tumors, surgery may not only be technically challenging, but it also may be associated with significant ocular morbidity, such as vision loss or ocular motility disturbances, or in rare cases it may be associated with mortality.^{1–9}

Imaging studies of the orbits, including computed to-

Table 1. Suggested Guidelines* for Interpretation of Orbital Computed Tomographic and/or Magnetic Resonance Imaging Studies

Location	Content	Soft Tissue Characteristics	Bone Characteristics	Associated Features
Orbit/cavernous anterior to posterior	CT Homogeneous cystic	Configuration Regular—oval	Primary bone	Nerve Perineural involvement
Anterior orbit preseptal	Fluid level	Irregular	Erosion/destruction	Nerve distribution
Periorbital superior	Gas/air calcification		Remodeling	
Periorbital inferior lacrimal sac	CT contrast enhance [†] Homogeneous enhancement	Margin characteristics Circumscribed	Hypertostosis Sphenoid wing/aplasia	Soft tissue SOV enlargement
Lacrimal fossa	CT—hypodense	Diffuse		EOM atrophy
Lateral orbit	CT—isodense			Fat stranding
Inferior orbit	CT—hyperdense	Relation to adjacent soft tissue		Ring enhancement
Inferomedial medial orbit		Molding—follows planes		Soft tissue destruction
Superior orbit	MR Fluid level	Globe indentation		Bone
Globe	Gas/air			Arising from
Intra-conal optic nerve	Flow void			Suture/dumbbell
Optic nerve sheath	MR contrast enhance [†]			Sunburst pattern
Orbital fat	Homogeneous enhancement			Ground glass
IR	Homogeneous T1			Periosteal involvement
MR	Inhomogeneous T1			Epidural extension
SR	Homogeneous T2			Widening of a foramen
LR	Inhomogeneous T2			Narrowing of a foramen
Panorbital	T1—hypointense			Paranasal sinuses
Inferior orbital fissure	T1—iso-intense			Sinus opacity
Superior orbital fissure	T1—hyperintense			Frontal sinus opacity
Apical	T2—hypointense			Ethmoid sinus opacity
Sphenoid wing	T2—iso-intense			Sphenoid sinus opacity
Cavernous sinus	T2—hyperintense			Maxillary
Bilateral				Destruction of sinuses
Adjacent				
Paranasal sinuses				
Temporal fossa				
Intracranial				
Meckel's cave				

CT = computed tomography; EOM = extraocular muscles; IR = inferior rectus; LR = lateral rectus; MR = medial rectus; SOV = superior orbital vein; SR = superior rectus.

*These guidelines were used to evaluate computed tomographic (CT) and/or magnetic resonance imaging (MRI) studies of 131 patients with orbital tumors that underwent orbital biopsy at the Jules Stein Eye Institute during a 4-year period. Features were divided according to five major criteria: (1) anatomic location, (2) content, (3) soft tissue, (4) bone characteristics, and (5) associated features. Brain gray matter was used as a point of reference to define density of the tumors by CT and intensity of the tumors by MRI.

[†]Homogeneous enhancement was marked as one distinct feature, whether enhancement was noticed in computed tomography or magnetic resonance imaging scan.

mography (CT) and magnetic resonance imaging (MRI) are the cornerstone of orbital diagnosis.^{10–23} These studies delineate the extent of the tumor and invasion to the orbit and its vicinity,²³ and often the results lead to suggestions of the biology of the disease process, narrowing the differential diagnosis and setting the stage for development of an appropriate treatment plan. In the vast majority of cases this will include obtaining a tissue biopsy. In most fields of ophthalmology, such as medical retina, there exist clear guidelines for interpretation of medical images (e.g., fluorescein angiography); these are taught during residency and fellowship and are utilized in the day-to-day practice. On the other hand, no common language for describing orbital imaging exists, even between orbital surgeons, general ophthalmologists, and other specialists, such as radiologists.

The purpose of the current study was to propose a terminology and systematic approach for interpretation of imaging studies of the orbits. We reviewed orbital imaging (CT and/or MRI) in patients with orbital tumors that underwent orbital biopsy at the Jules Stein Eye Institute during a

4-year period. From a list of potential characteristics, we hope to identify several distinct features that can be used as predictive indicators for the nature of the orbital disease prior to obtaining a tissue diagnosis, and which may form the basis for a future prospective study.

Patients and Methods

Patients

A retrospective medical chart review of all patients diagnosed with orbital tumors who underwent orbital biopsy at the Jules Stein Eye Institute in January 2000 to December 2003 was performed. All patients had a definitive clinical diagnosis that was confirmed by histological evaluation of the biopsy.

Methods

Guidelines for reading orbital imaging were established by experienced orbital surgeons and neuroradiologists, and an 84-feature

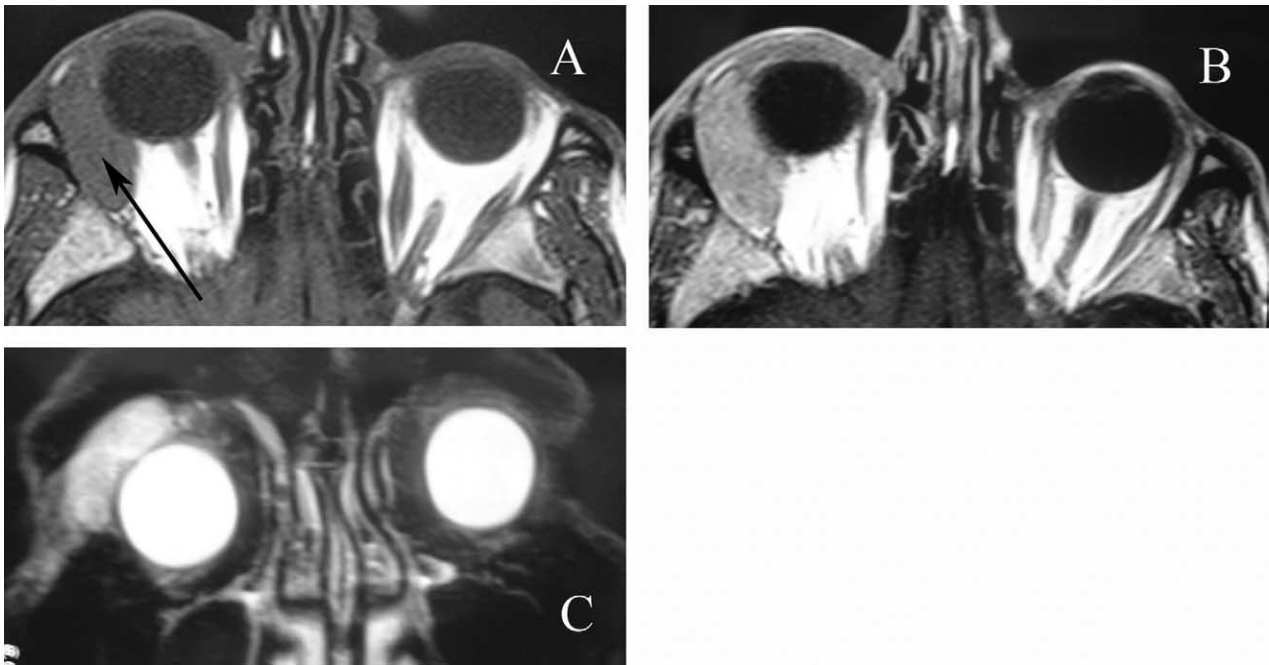


Figure 1. Magnetic resonance imaging (MRI) scan of the orbit of an 80-year old patient presenting with right side proptosis. **A**, T1-weighted sequence, precontrast, revealing a well-defined, circumscribed, superotemporal orbital mass located in the lacrimal fossa (black arrow). The lesion is isointense to brain gray matter and is molding around orbital structures. No bone destruction or bone erosion is noticed. **B**, Gadolinium enhanced T1-weighted sequence, axial section, showing homogeneous enhancement of the lesion. **C**, The lesion is hyperintense on T2-weighted sequence, coronal section. Orbital biopsy of the lesion demonstrated lymphoma. The following features were marked as positive (1): lacrimal fossa, circumscribed, molding, isointense T1, hyperintense T2, MRI contrast enhancement, and homogeneous enhancement.

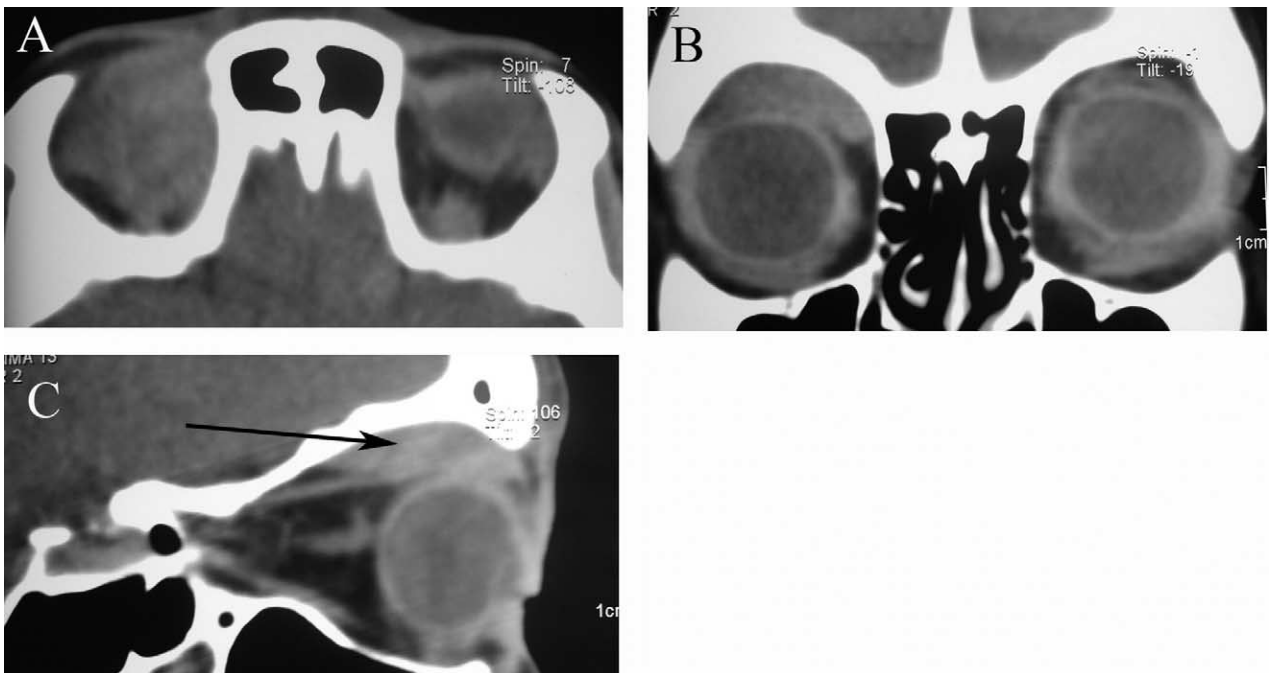


Figure 2. Computed tomographic (CT) scans of the orbit of a 35-year-old female with a history of non-Hodgkin's lymphoma and a recent onset of right orbital mass. **A**, Axial section through the superior orbit showing the lesion to occupy the patient's superior orbital space. **B**, Computerized tomographic scan of the orbit showing right superior orbital homogeneous lesion, which is molding around the globe and is not associated with destructive features. **C**, Sagittal section showing the anterior-posterior extent of the lesion and the extraconal location (black arrow). Orbital biopsy was consistent with the diagnosis of orbital non-Hodgkin's lymphoma. The following imaging characteristics were assigned: superior orbit, extraconal, circumscribed, homogeneous, molding, CT isodense, CT contrast enhancement, and homogeneous enhancement.

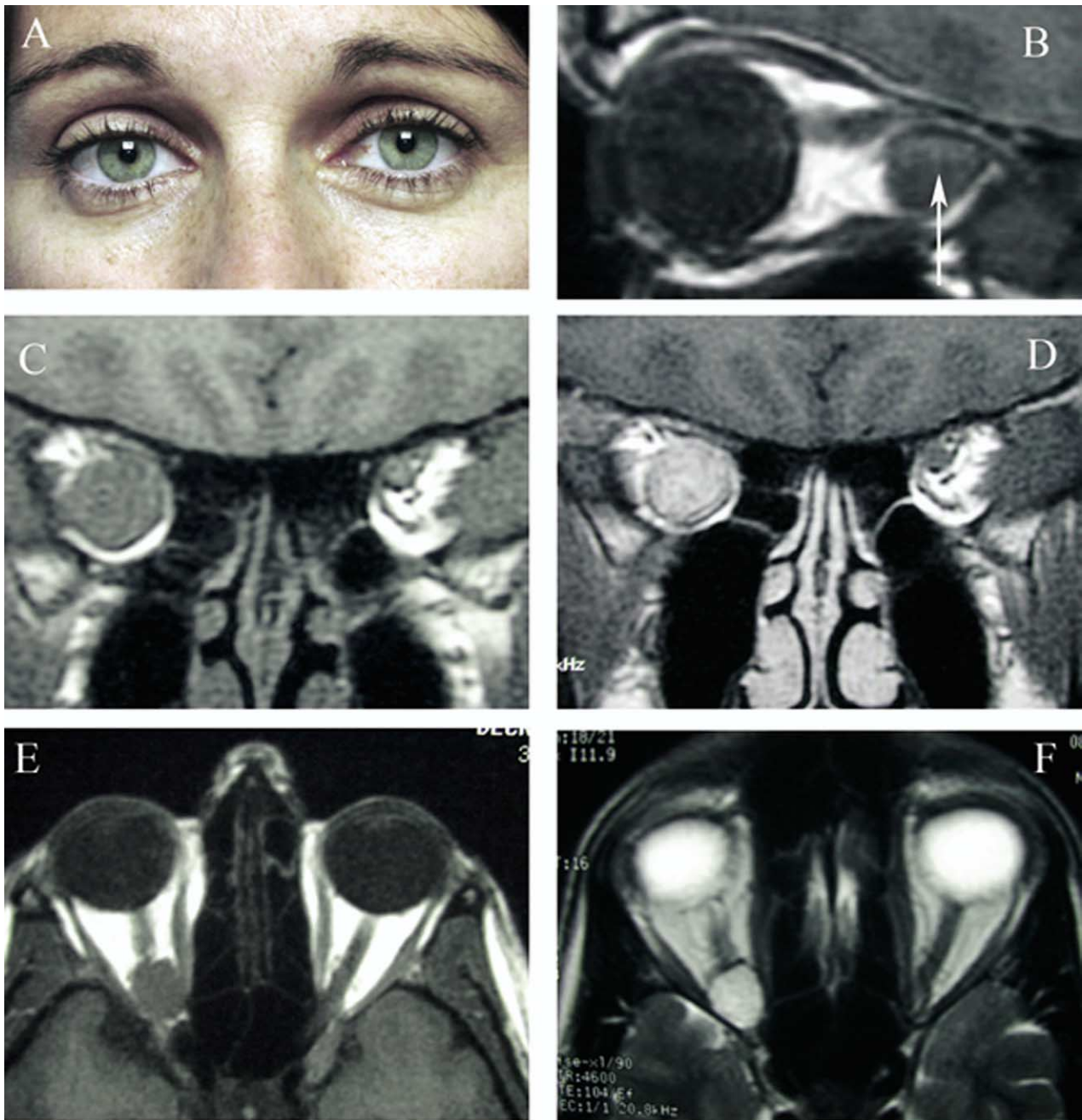


Figure 3. **A**, A 32-year-old female with a history of right orbital intraconal tumor was referred for evaluation of optic nerve dysfunction. Clinical examination revealed right eye proptosis and mild right upper eyelid ptosis. **B**, Magnetic resonance imaging (MRI) scan of the orbit, T1-weighted image, sagittal section, showing right intraconal lesion, round or oval in shape, hypointense to brain gray matter (white arrow). **C**, T1-weighted image, coronal section, precontrast showing the homogeneous lesion. **D**, T1-weighted image with gadolinium, coronal section, showing homogeneous enhancement of the orbital mass. **E**, T1-weighted image, axial section, showing the apical location of the tumor. **F**, T2-weighted sequence, showing hyperintensity of the intraconal mass. The patient underwent excisional biopsy of the lesion, and histopathology was consistent with cavernous hemangioma. The following imaging features were assigned: intraconal, apex, round/oval, T1 hypointense, T2 hyperintense, MRI contrast enhancement, and homogeneous enhancement.

table was built, based on anatomical location, content, soft tissue, and bone characteristics (Table 1). Using this table, all patient scans (including CT and/or MRI) were reevaluated in an unmasked fashion by 3 different observers (i.e., a fellow in orbital and ophthalmic plastic surgery, a fellow in neuroradiology, and a second-year ophthalmology resident). Positive features for each of the scans were recorded. If the feature existed, it was marked as a

1, otherwise it was marked as a 0; multiple features could be assigned to the imaging study as required. Brain gray matter was used as a point of reference to define density of the tumors by CT and intensity of the tumors by MRI. We relate the most significant characteristics, because some locations and features are redundant (Figs 1–5).

At a later stage, we calculated which of the multiple features

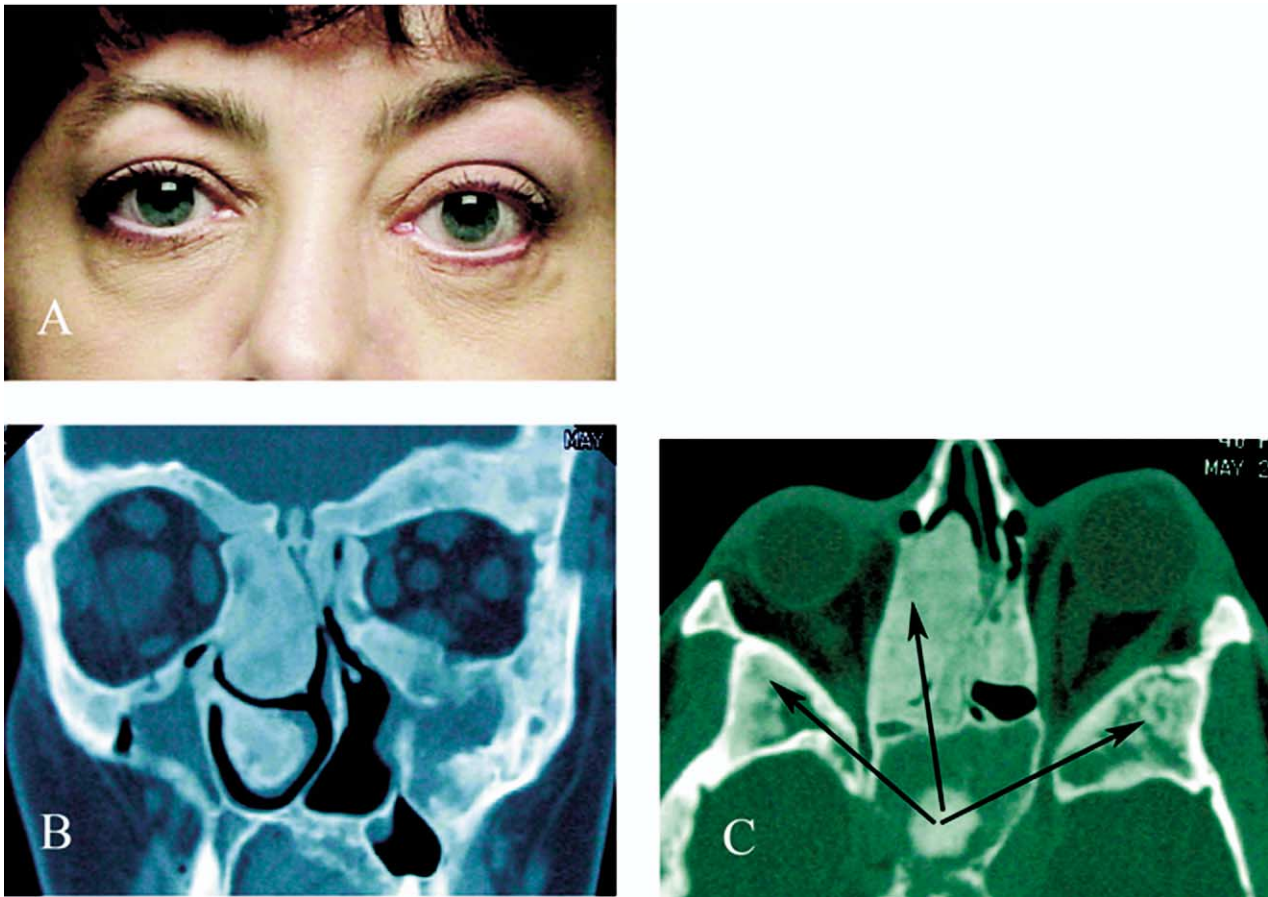


Figure 4. A, A 40-year-old woman with a diagnosis of fibrous dysplasia was referred for evaluation of left proptosis and decreased optic nerve function. B, Computed tomographic (CT) scan of the orbits, coronal section, showing diffuse bone involvement of all orbital walls along with maxillary bones in a ground-glass appearance. C, Computed tomographic scan of the orbit, axial section, showing obliteration of ethmoidal sinuses by the process, enlarged trigone space and narrowing of the superior orbital fissure on the left (black arrows). The patient underwent surgical debulking of the tumor on the left side. The following imaging features were assigned: primary bone, bilateral involvement, bone remodeling with narrowing of a foramen, CT hypodense and CT hyperdense, and diffused and ground-glass appearance.

had a significant differential ability to discriminate between benign, malignant, and inflammatory lesions of the orbits, and which of the features did not add any information in that regard. Finally, sensitivity, specificity, and positive- and negative-predictive values for malignant or benign lesions were calculated. The study was approved by the local institutional review board.

Statistical Analysis

Statistical analysis was performed using statistical software (SAS version 8.2, Cary, NC) and a P value of <0.05 was considered statistically significant. Chi-square tests were used to assess the relationships between qualitative measurements, such as type of diagnosis and features of various tests. All P values reflect the differences among 3 diagnosis types: (1) benign, (2) malignant, and (3) inflammatory. The Kruskal-Wallis-Wilcoxon tests were used for continuous variables, such as age and number of features, and the Fisher exact test was used for all other variables (i.e., categorical variables). The Fisher exact test was performed when sample size in the subgroups was deemed too small. The κ statistics were calculated to evaluate the agreement between different features of the tests.

Results

One hundred thirty-one patients (64 males and 67 females; mean age of 51 years) with orbital tumors that underwent orbital biopsy were included in the study.

On average, a patient had $9 (\pm 3)$ positive features when all 84 features were considered. The smallest number of positive features simultaneously found in a single patient was 3, and the largest number of features simultaneously found in a single patient was 22. The malignant group had a slightly higher average number of positive features found (i.e., $10.1 [\pm 3.2]$) than the other 2 groups, but the difference was not statistically significant ($P = 0.085$).

Fifty percent of all tumors were benign, and the rest were divided evenly between malignant and inflammatory lesions (Table 2). No gender differences were found between the different groups. Patients with malignant tumors were significantly older (mean age, 67 years compared with 43 and 48 years in the benign and inflammatory groups, respectively). Table 3 describes the clinical features of patients with orbital tumors participating in the study.

Each of the imaging features was evaluated separately for occurrence in 3 major diagnoses groups: (1) malignant, (2) benign,

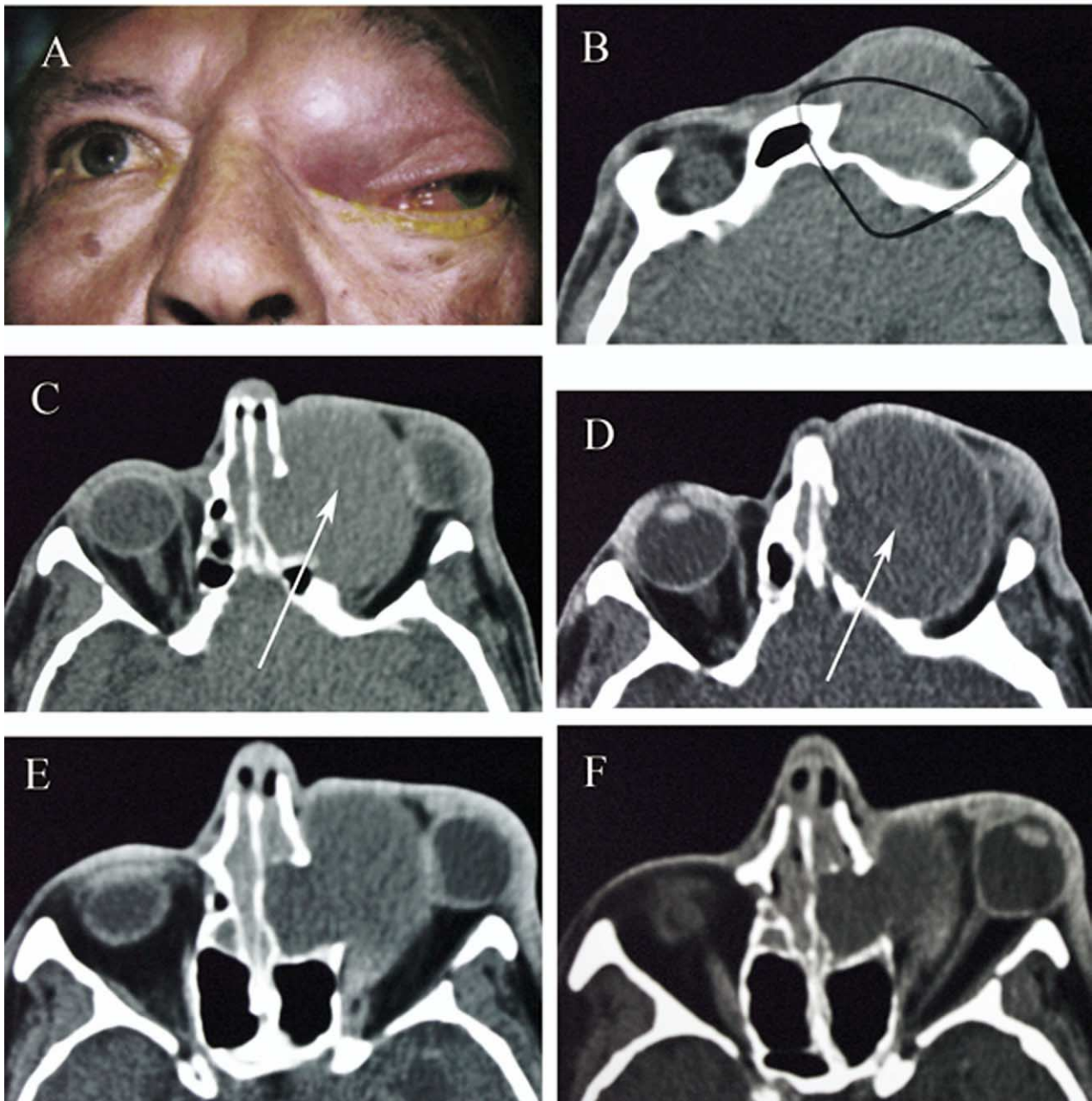


Figure 5. A, A 65-year-old man with a history of gradual onset left proptosis and inferolateral displacement. B–F, Computed tomographic (CT) scans of the orbits and paranasal sinuses. B, Axial section showing frontal bone erosion by the lesion (circle). C, Precontrast section showing large medial orbital homogeneous mass and ethmoid sinus opacity (white arrow). D, Postcontrast image showing rim enhancement (white arrow). E, Axial section showing the mass indenting the left globe. F, Axial section showing left globe tenting by marked anterior displacement. The lesion was diagnosed as frontal mucocele; the patient underwent successful drainage of the mucocele with tube placement. The following imaging features were assigned: paranasal sinuses, sinus opacity frontal, sinus opacity ethmoidal, bone erosion, circumscribed, CT homogeneous, CT isodense, and CT contrast rim enhancement.

and (3) inflammatory. Only features with ≥ 5 occurrences were evaluated in the statistical analysis using Fisher exact test (i.e., on average 9 or 10 features were evaluated for each group). Circumscribed shape was the most common feature overall (65%), and it was the most common feature in benign tumors (74%); MRI contrast enhancement was the most common feature in malignant tumors (60%), whereas irregular shape was the most common

feature in inflammatory lesions (65%). The second most common features were MRI contrast enhance for all lesions (50%) and for benign tumors (40%); inflammatory processes (58%) and circumscribed shape and anterior orbit location were the most common features for malignant tumors (54%).

Nineteen distinct imaging features showed a significantly different prevalence among the 3 groups (Table 4, Fig 6).

Table 2. Diagnosis of 131 Patients Presenting with Orbital Tumor at the Jules Stein Eye Institute during a 4-Year Period*

Disease/Diagnosis	Total (%)
Hemangioma	10 (7.6)
Meningioma	8 (6.1)
Choristoma/dermoid/cyst	7 (5.4)
Fibrous dysplasia	7 (5.3)
Pleomorphic adenoma	6 (4.6)
Active vascular	6 (4.6)
Neurofibroma	5 (3.8)
Osteoma	5 (3.8)
Schwannoma	4 (3.1)
Meningioma	1 (0.8)
Lipoma/dermatolipoma	1 (0.8)
Neuroma	1 (0.8)
Glioma	1 (0.8)
Erdheim-Chester	1 (0.8)
Squamous papilloma	1 (0.8)
Total benign	65
Idiopathic inflammation	27 (20.6)
Mucocele	4 (3.1)
Total inflammatory	31
MALT/lymphoma	12 (9.2)
Basal cell carcinoma	5 (3.8)
Squamous cell carcinoma	5 (3.8)
Adenocystic carcinoma lacrimal	4 (3.1)
Malignant melanoma	2 (1.5)
Spindle cell carcinoma	2 (1.5)
Adenocarcinoma	1 (0.8)
Sebaceous carcinoma	1 (0.8)
Osteogenic sarcoma	1 (0.8)
Metastasis	1 (0.8)
Neuroblastoma/esthesioneuroblastoma	1 (0.8)
Total malignant	35
Total of all types	131

MALT = mucosa-associated lymphoid tissue.

*All patients underwent orbital biopsy of the lesions for tissue diagnosis.

Tumors in the lacrimal fossa or the anterior orbit were more likely to be malignant or inflammatory; panorbital tumors or tumors involving the orbital fat were always benign or inflammatory, and this was also the case when hyperostosis was noted. Although bone erosion was significantly more common in malignant tumors, it was also found in benign and inflammatory lesions. Frontal sinus opacity was associated with a malignant or inflammatory process rather than a benign orbital lesion. Malignant lesions were also found to be more irregular in shape, molding around normal orbital structures, diffuse in nature, and associated with perineural involvement. Benign lesions were clearly more circumscribed and oval in comparison with tumors in the other 2 groups; interestingly, none of the malignant or inflammatory lesions was found to be oval. Regarding image intensity, malignant tumors were more isointense on T2--sequence, and benign or inflammatory lesions were more hyperintense on T2. Regarding image density, benign tumors were either hyperdense or hypodense on CT scan compared with malignant or inflammatory.

None of the features had a high sensitivity for diagnosing malignant versus benign processes. Features like panorbital involvement, orbital fat, frontal sinus opacity, molding around orbital structures, perineural involvement, and fat stranding had specificity of 97% to 100%, and the latter had a positive predictive value of 100% (Table 5). Similar values were calculated when including benign and inflammatory lesions in the same group and then comparing them with malignant processes (data not shown).

The following features had a marginal difference ($P < 0.1$ and $P > 0.05$) between the 3 groups: tumors involving paranasal sinuses were more likely to be inflammatory or malignant; bone remodeling was more likely to be identified as a benign, slow-growing process; contrast enhancement on MRI scan was more prevalent in malignant and inflammatory lesions; and finally ground-glass appearance of bone was only prevalent in fibrous dysplasia (Table 6).

We calculated κ values for all imaging features to filter the features that are likely to have the same value; for this we used a cut off of $\kappa > 0.5$, as shown in Table 6. Negative κ means that

Table 3. Clinical Features of 131 Patients with Orbital Tumors That Underwent Orbital Biopsy at the Jules Stein Eye Institute during a 4-Year Period

	Overall		Type of Tumor						P Value
			Benign		Malignant		Inflammatory		
	N	%	N	%	N	%	N	%	
No. of Patients	131		65		35		31		
Gender									0.615
Male	64	49	29	45	19	54	16	52	
Female	67	51	36	55	16	46	15	48	
Age (yrs)	50.8±21.9		43.1±18.8		67.1±16.0		48.4±24.3		<0.001
Side									0.113
Right	65	50	38	58	12	34	15	48	
Left	59	45	23	35	22	63	14	45	
Bilateral	7	5	4	6	1	3	2	6	
Type									
Benign	65	50							
Malignant	35	27							
Inflammatory	31	24							
MRI (yes)	86	66	42	65	24	69	20	65	0.942
CT (yes)	64	49	33	51	16	46	15	48	0.923
No. of features (±SD)	9.1±3.2		8.7±2.4		10.1±3.2		8.9±4.4		0.085

CT = computed tomography; MRI = magnetic resonance imaging; SD = standard deviation.

Imaging studies of all patients. Computed tomographic and/or magnetic resonance imaging were evaluated for all patients by 3 unmasked observers.

Table 4. Imaging Features with Significant ($P < 0.05$) Difference of Occurrence between Benign, Malignant, and Inflammatory Lesions among 131 Patients with Biopsy-Proven Orbital Tumors*

	Overall		Type of Tumor						P Value
			Benign		Malignant		Inflammatory		
	N	%	N	%	N	%	N	%	
No. of Patients	131		65		35		31		
Tumor location									
Panorbital	9	7	2	3	0	0	7	23	<0.001
Orbital fat	6	5	0	0	0	0	6	19	<0.001
Lacrimal fossa	24	18	6	9	10	29	8	26	0.022
Anterior orbit preseptal	41	31	13	20	19	54	9	29	0.002
Sphenoid wing	13	10	11	17	2	6	0	0	0.02
Sinus opacity frontal	10	8	1	2	3	9	6	19	0.006
Bone characteristics									
Hyperostosis	15	11	14	22	0	0	1	3	<0.001
Primary bone	14	11	13	20	1	3	0	0	0.002
Erosion	20	15	4	6	11	31	5	16	0.004
Content*									
T2-isointense	20	15	8	12	10	29	2	6	0.039
T2-hyperintense	34	26	25	38	4	11	5	16	0.005
CT-hypodense	7	5	7	11	0	0	0	0	0.033
CT-hyperdense	10	8	10	15	0	0	0	0	0.003
Soft tissue characteristics									
Regular-oval	19	15	19	29	0	0	0	0	<0.001
Diffuse	41	31	10	15	15	43	16	52	<0.001
Molding	12	9	2	3	10	29	0	0	<0.001
Circumscribed	80	61	48	74	19	54	13	42	0.007
Irregular	58	44	20	31	18	51	20	65	0.005
Associated features									
Fat stranding	5	4	0	0	0	0	5	16	<0.001
Perineural involvement	6	5	0	0	4	11	2	6	0.015
Nerve distribution	7	5	7	11	0	0	0	0	0.033

CT = computed tomography.

P values were calculated using Fisher exact test.

*Intensity (magnetic resonance imaging) and density (computed tomography) were graded relative to brain gray matter.

if the value of one variable is 1, then the other variable is likely to be 0.

Although some of the relationships are intuitive, such as optic nerve sheath and dural tail in optic nerve sheath meningioma ($\kappa = 1.0$) or circumscribed and diffuse ($\kappa = -0.71$), others may be more intriguing, such as involvement of the superior orbital fissure or Meckel's cave associated with extraocular muscle atrophy ($\kappa = 0.66$) or periosteal involvement associated with opacity of the maxillary sinus (0.65). The clinical relevance of these associations, if real, remains to be examined.

Discussion

We propose guidelines to interpret orbital imaging studies, and we used these guidelines to analyze imaging studies of 131 patients with biopsy-proven orbital tumors. These guidelines are based on 5 major characteristics including anatomic location, content, soft tissue and bone characteristics, and associated features. We have found that some of the imaging features are associated with a more malignant process, such as irregular shape, molding around normal orbital structures, diffuse

in nature, perineural involvement, and bone erosion. Other features such as oval shape, hyperostosis, hyperintensity on T2, and hyperdensity or hypodensity on CT are likely to characterize benign tumors. Primary bone lesions were more likely to be benign in the current study (20% of all benign vs. 3% of all malignant tumors). Inflammatory lesions showed panorbital or orbital fat involvement and fat stranding; these features were not noticed in benign or malignant lesions. Similar to malignant tumors, inflammatory lesions were found to be more diffuse and irregular rather than oval or circumscribed. However, none of the imaging features had a high sensitivity to distinguish between malignant, benign, and inflammatory tumors. This may be a reflection of the relatively small sample size, and the fact that some of the features occurred in a small number of patients. To be able to focus on the most clinically relevant features, we have only included imaging features with occurrence of at least 5 in the statistical analysis.

It is well known that thoughtful analyses of CT and MRI imaging of the orbit, paired with careful history and clinical examination, along with careful observation, are critical elements in orbital diagnosis.^{5,6,10-12,16,22}

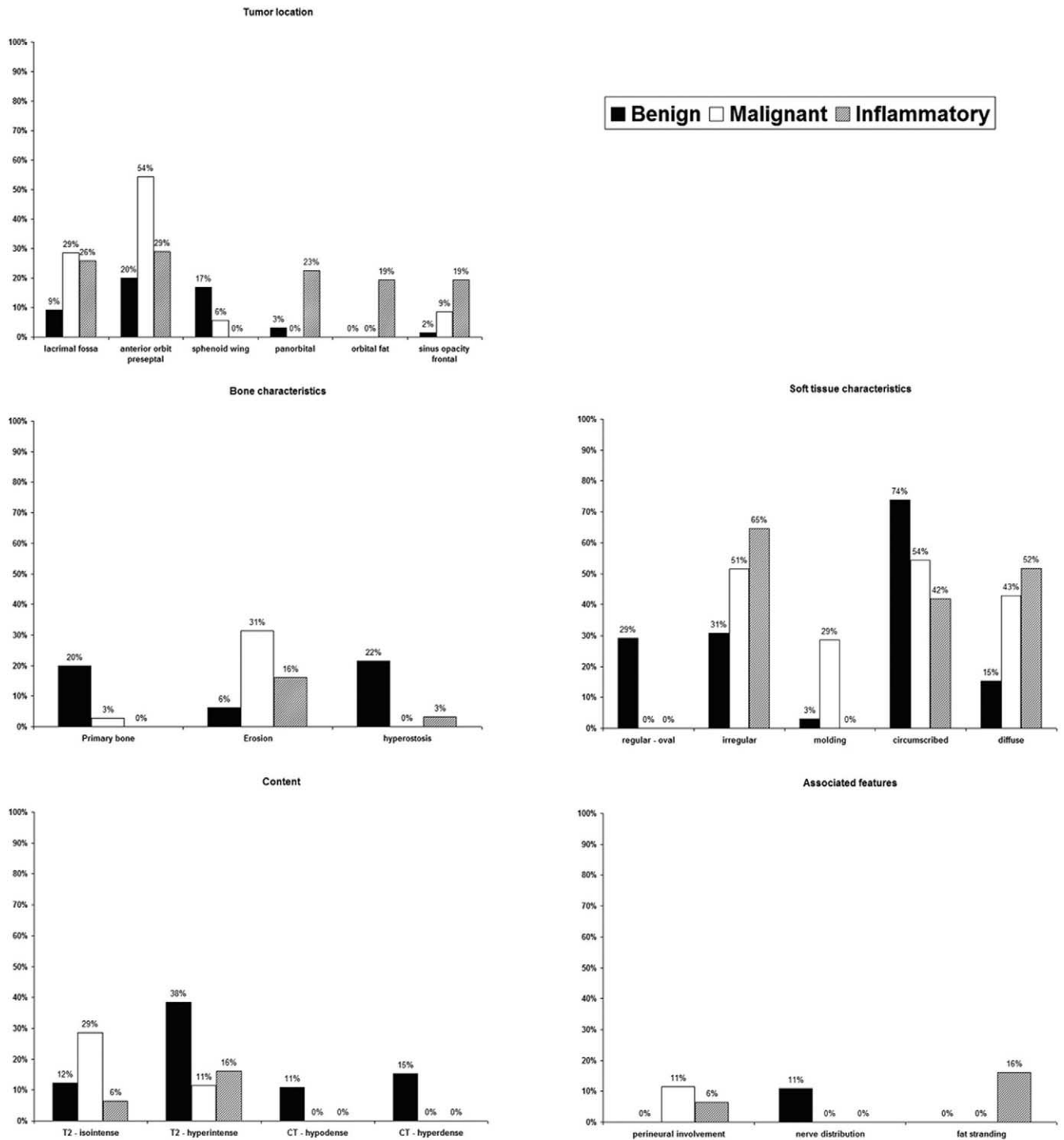


Figure 6. Imaging features with significant difference ($P < 0.05$) of occurrence between benign, malignant, and inflammatory lesions among 131 patients with biopsy-proven orbital tumors. P values were calculated using the Fisher exact test.

Clearly, the more accurate our interpretation of orbital imaging studies, the more logical, efficient, and minimally invasive will be our subsequent treatment plan. In a retrospective fashion, Eisen et al²³ explored the predictive value of preoperative imaging in orbital invasion by tumors of the paranasal sinuses. They found that the most

sensitive predictor of orbital invasion was a tumor located adjacent to the periorbita; extraocular muscle involvement and orbital fat obliteration had the highest positive predictive values (100% and 80%, respectively). They concluded that imaging studies should be used in surgical planning and cannot replace intraoperative as-

Table 5. Positive Predictive Values, Negative Predictive Values, Sensitivity, and Specificity of Imaging Features in Evaluating Malignant versus Benign Processes (Excluding Inflammatory Lesions) in Patients with Orbital Tumors*

	Benign vs. Malignant (Excluding Inflammatory)							
	Positive Predictive Value [†]		Negative Predictive Value [‡]		Sensitivity [§]		Specificity	
	n	%	n	%	n	%	n	%
No. of patients					35		65	
Orbital fat	0	NA	65	65	0	0	65	100
Perineural involvement	4	100	65	68	4	11	65	100
Fat stranding	0	NA	65	65	0	0	65	100
Sinus opacity frontal	3	75	64	67	3	9	64	98
Panorbital	0	0	63	64	0	0	63	97
Molding	10	83	63	72	10	29	63	97
Erosion	11	73	61	72	11	31	61	94
Lacrimal fossa	10	63	59	70	10	29	59	91
Nerve distribution	0	0	58	62	0	0	58	89
CT-hypodense	0	0	58	62	0	0	58	89
T2-isointense	10	56	57	70	10	29	57	88
CT-hyperdense	0	0	55	61	0	0	55	85
Diffuse	15	60	55	73	15	43	55	85
Sphenoid wing	2	15	54	62	2	6	54	83
Primary bone anterior orbit	1	7	52	60	1	3	52	80
Preseptal	19	59	52	76	19	54	52	80
Hyperostosis	0	0	51	59	0	0	51	78
Regular-oval	0	0	46	57	0	0	46	71
Irregular	18	47	45	73	18	51	45	69
T2-hyperintense	4	14	40	56	4	11	40	62
Circumscribed	19	28	17	52	19	54	17	26

NA = not available.

*Only features with significantly different occurrence between malignant and benign groups were included in the calculation.

[†]Rate of detecting disease among patients with positive test results equals number of patients with disease (malignant) and positive test results per number of patients with positive test results.

[‡]Rate of detecting nondisease among patients without positive test results equals number of patients without disease (malignant) and negative test results per number of patients with negative results.

[§]Rate of positive test results among patients with disease equals number of patients with disease (malignant) and positive test results per number of patients with disease (malignant).

^{||}Rate of negative test results among patients without disease equals number of patients without disease (malignant) and negative test results per number of patients without disease (malignant).

assessment in cases of suspected orbital invasion. Their group included 19 CT and 17 MRI scans from patients at risk for orbital invasion. Interestingly, in our series, orbital fat had a specificity of 100%, implying that tumors not involving or obliterating the orbital fat were likely to be benign. Our group of patients was more heterogeneous and focused on orbital instead of paranasal sinus disease, and this included a wider variety of diagnoses, but the nature of the biologic behavior can be compared.

Benign lesions in our study were found to be well circumscribed, oval in shape, hyperintense on T2, and hypodense or hyperdense on CT; cavernous hemangioma was the most frequent diagnosis in that group (>30%) and may have contributed the most in analyzing imaging characteristics in that group. Our results are in line with previous studies that have analyzed MRI findings in cavernous hemangioma.¹³ They have found these lesions to be a well-defined, intraconal, homogeneous mass, isointense to muscle on T1, and hyperintense on T2 with progressive filling on a gadolinium-enhanced sequence.

Polito et al¹⁹ investigated MRI and CT characteristics of orbital lymphomas and correlated these findings to

clinical signs. Imaging showed round or lobulated masses, molding to adjacent structures, and a wedge-shaped enlargement of the lacrimal gland; only 35% of all lymphoid tumors were hyperintense on T2. In our study, orbital lymphoma comprised more than one third of all malignant tumors, and we describe similar image findings, even though malignant tumors in our study were more isointense on T2, whereas inflammatory lesions were more hyperintense on T2 sequenced images. It is known, however, that inflammatory presentation is not uncommon in orbital lymphoid tissue, and this can explain the image intensity in their study.

Ultrasound with Doppler evaluation of the orbit provides unique diagnostic information in patients with an orbital mass; its major advantage over CT or MR scans is that it can obtain dynamic information, is readily available in many ophthalmic centers, and does not expose patients to radiation. However, expertise in interpretation is not widespread, and its use as a diagnostic tool in orbital tumors is limited.^{24,25}

The study is limited by the small sample size. Additional features would probably be taken into account had we included more patients in the study, since imaging

Table 6. Imaging Features with Similar Predictive Values of Computed Tomographic and/or Magnetic Resonance Imaging Studies of 131 Patients with Biopsy-Proven Orbital Tumors*

Feature 1	Feature 2	Kappa
Optic nerve sheath	Dural tail	1.00
Sphenoid wing	Primary bone	0.71
Circumscribed	Diffuse	-0.71
Homogeneous T1 [†]	Homogeneous T2	0.69
Superior orbital fissure	EOM atrophy	0.66
Meckel's cave	EOM atrophy	0.66
Periosteal involvement	Sinus opacity maxillary	0.65
Panorbital	Orbital fat	0.65
Heterogeneous T1	Heterogeneous T2	0.64
Sinus opacity frontal	Sinus opacity ethmoid	0.64
MRI contrast enhancement	T1-isointense	0.59
Primary bone	Hyperostosis	0.57
Inferomedial	Lacrimal sac	0.56
LR	Orbital fat	0.53
Sphenoid wing	Hyperostosis	0.52
Hyperostosis	CT-hyperdense	0.52
Homogeneous T1	T1-isointense	0.51

CT = computed tomography; EOM = extraocular muscle; LR = lateral rectus; MRI = magnetic resonance imaging.

*Table shows features with κ values higher than 0.5; (negative Kappa means that if the value of one variable is 1 the other variable is likely to be 0).

[†]Intensity (magnetic resonance imaging) and density (computed tomography) were graded relative to brain gray matter.

features with occurrence of less than 5 were not included in statistical comparison. Including a larger group of tumors may have enabled us to find imaging features with a higher specificity for distinguishing benign versus malignant processes. Tumors included in the study reflect the referral pattern to our orbital clinic, and each institution has its own unique spectrum of orbital disease.

The significance of creating defined guidelines for reading and analyzing orbital imaging studies extends beyond the need to isolate distinct features with a significant predictive estimate of the nature of the biological process. It is of obvious value to create a common language among radiologists, orbital surgeons, and general ophthalmologists. These guidelines, if confirmed in other studies, may also be used in teaching residents and fellows, with an emphasis on establishing a systematic method of evaluating CT and MRI of the orbit. Although we recognize that the table we created may not be all-encompassing, we did find the classification presented in this study easy to use, particularly because it is based on logical anatomical and radiological features. We hope it will stimulate ongoing dialogue that could lead to a systematic approach and common descriptive language for interpretation of orbital imaging studies.

We are engaged in a prospective study in which we will evaluate radiographic images prior to orbital biopsy using our table, with an emphasis on features that were significantly different between all 3 groups of tumors. Prospective studies will likely provide more accurate data on the true sensitivity, positive predictive value, and negative predictive value of the various imaging features. The logical thought process that characterizes the elegant

diagnosis of orbital disease is the stimulating exercise that draws many practitioners to the field of orbital surgery. Advances in our ability to interpret orbital imaging allow optimization of the decision-making tree, defining the most efficient and least invasive pathways toward helping our patients with their disease.

References

- Demirci H, Shields CL, Shields JA, et al. Orbital tumors in the older adult population. *Ophthalmology* 2002;109:243-8.
- Eldrup-Jorgensen P, Fledelius H. Orbital tumours in infancy. An analysis of Danish cases from 1943-1962. *Acta Ophthalmol (Copenh)* 1975;53:887-93.
- Goldberg RA, Rootman J, Cline RA. Tumors metastatic to the orbit: a changing picture. *Surv Ophthalmol* 1990;35:1-24.
- Henderson JW, Campbell RJ, Farrow GM, Garrity JA. *Orbital Tumors*. 3rd ed. New York: Raven Press; 1994:43-52.
- Johansen S, Heegaard S, Bogeskov L, Prause JU. Orbital space-occupying lesions in Denmark 1974-1997. *Acta Ophthalmol Scand* 2000;78:547-52.
- Rootman J, Chang W, Jones D. Distribution and differential diagnosis of orbital disease. In: Rootman J, ed. *Diseases of the Orbit: A Multidisciplinary Approach*. Philadelphia: Lippincott Williams & Wilkins; 1988:53-84.
- Shields JA, Bakewell B, Augsburger JJ, et al. Space-occupying orbital masses in children. A review of 250 consecutive biopsies. *Ophthalmology* 1986;93:379-84.
- Shields JA, Bakewell B, Augsburger JJ, Flanagan JC. Classification and incidence of space-occupying lesions of the orbit. A survey of 645 biopsies. *Arch Ophthalmol* 1984;102:1606-11.
- Seregard S, Sahlin S. Panorama of orbital space-occupying lesions. The 24-year experience of a referral centre. *Acta Ophthalmol Scand* 1999;77:91-8.
- Gorospe L, Royo A, Berrocal T, et al. Imaging of orbital disorders in pediatric patients. *Eur Radiol* 2003;13:2012-26.
- Brun V, Lafitte F, Hamedani M, et al. How to investigate a patient with exophthalmos? [in French]. *J Neuroradiol* 2002;29:161-72.
- McCaffery S, Simon EM, Fischbein NJ, et al. Three-dimensional high-resolution magnetic resonance imaging of ocular and orbital malignancies. *Arch Ophthalmol* 2002;120:747-54.
- Thorn-Kany M, Arrue P, Delisle MB, et al. Cavernous hemangiomas of the orbit: MR imaging. *J Neuroradiol* 1999;26:79-86.
- Valvassori GE, Sabnis SS, Mafee RF, et al. Imaging of orbital lymphoproliferative disorders. *Radiol Clin North Am* 1999;37:135-50.
- Wenig B, Mafee MF, Ghosh L. Fibro-osseous, osseous, and cartilaginous lesions of the orbit and paraorbital region. Correlative clinicopathologic and radiographic features, including the diagnostic role of CT and MR imaging. *Radiol Clin North Am* 1998;36:1241-59.
- Kaufman LM, Villablanca JP, Mafee MF. Diagnostic imaging of cystic lesions in the child's orbit. *Radiol Clin North Am* 1998;36:1149-63, xi.
- Maya MM, Heier LA. Orbital CT. Current use in the MR era. *Neuroimaging Clin N Am* 1998;8:651-83.
- Duvoisin B, Zanella FE, Sievers KW. Imaging of the normal and pathological orbit. *Eur Radiol* 1998;8:175-88.
- Polito E, Galienu P, Leccisotti A. Clinical and radiological presentation of 95 orbital lymphoid tumors. *Graefes Arch Clin Exp Ophthalmol* 1996;234:504-9.

20. Warner MA, Weber AL, Jakobiec FA. Benign and malignant tumors of the orbital cavity including the lacrimal gland. *Neuroimaging Clin N Am* 1996;6:123–42.
21. Friedman DP, Rao VM, Flanders AE. Lesions causing a mass in the medial canthus of the orbit: CT and MR features. *AJR Am J Roentgenol* 1993;160:1095–9.
22. Hopper K, Sherman JL, Boal DK, Egli KD. CT and MR imaging of the pediatric orbit. *Radiographics* 1992;12:485–503.
23. Eisen MD, Yousem DM, Loevner LA, et al. Preoperative imaging to predict orbital invasion by tumor. *Head Neck* 2000;22:456–62.
24. Jain R, Sawhney S, Berry M. Real-time sonography of orbital tumors, colour Doppler characterization: initial experience. *Acta Ophthalmol Suppl* 1992;(204):46–9.
25. Glasier C, Brodsky MC, Leithiser RE Jr, et al. High resolution ultrasound with Doppler: a diagnostic adjunct in orbital and ocular lesions in children. *Pediatr Radiol* 1992;22:174–8.